Paddlebots: Translation of rotating colloidal assemblies near an air/water interface

E. Wolvington¹, L. Yeager¹, Yan Gao², C.J. Zimmermann¹, D.W.M. Marr^{1,*}

¹Department of Chemical and Biological Engineering, Colorado School of Mines, Golden, CO

80401, USA

²Materials Science and Engineering, Colorado School of Mines, Golden, CO, 80401, USA

*Corresponding author: dmarr@mines.edu

Abstract

Microbot propulsion requires unique strategies due to the dominance of viscosity and the

reversible nature of microscale flows. To address this, swimmers of specific structure that

translate in bulk fluid are commonly used; however, another approach is to take advantage of the

inherent asymmetry of liquid/solid surfaces for microbots (µbots) to walk or roll. Using this

technique, we have previously demonstrated that superparamagnetic colloidal particles can be

assembled into small ubots which can quickly roll along solid surfaces. In an analogous

approach, here we show that symmetry can be similarly broken near air/liquid interfaces and

μbots propelled at rates comparable to those demonstrated for liquid/solid interfaces.

Introduction

Propulsion at the air water interface often involves swimming or rowing, transport methods

associated with turbulent flows and high Reynolds number fluid mechanics (1, 2). At the

microscale however, movement requires different considerations due to the reversible nature of

microfluidic flows. Familiar macroscale swimming and rowing methods are not effective and

specific designs, namely helical structures or flexible oars, are used to facilitate movement (3–6).

In an alternative approach that facilitates fabrication, we have previously demonstrated that

1

superparamagnetic colloidal particles can be assembled with a rotating magnetic field into spinning wheel-shaped structures (7–10). As these microwheels (μwheels) approach a solid surface, symmetry is broken and rotating μwheels roll along surfaces at high speeds (Fig 1A). With reorientation of the rotating magnetic field, μwheels can be readily redirected and driven to desired locations. Here we show that air/water interfaces can similarly be used to break symmetry and propel colloidal assemblies similar to μwheels, now paddlebots, near the liquid surface where classical rowing would not be effective.

At the air/water interface, surface tension can be dominant as demonstrated by water striders that can not only stay suspended on the liquid surface but also use differential surface indentation to translate (11–13). Similarly, gravity-induced surface depression can be used to create capillary forces to assemble surface bound colloids (14–16). As these studies demonstrate, at small length scales surfaces forces can dominate and can pin colloidal particles at interfaces (17, 18). To avoid trapping assembled paddlebots at the interface in our investigations, we instead use systems fully immersed in the fluid phase but near enough to the interface to experience differential drag. Our approach is illustrated in Fig 1B where an inverted geometry is used to suspend a fluid droplet containing superparamagnetic colloids which settle under the presence of gravity towards the air/water interface and, with available surfactant, remain within the liquid phase.

Experimental Section

Solution Preparation. Samples were prepared by first diluting 2 μ L of stock Dynabead solution (Dynabeads® M-450 Epoxy, Thermo Fisher, density = 1.6 g/cm³ (19), concentration = $4 \cdot 10^8$

beads/mL, and measured ζ potential of -55 mV (ZetaPALS, Brookhaven Instruments)) with 1 mL of 0.15% sodium dodecyl sulfate (SDS) (Sigma-Aldrich). Fifteen μL droplets containing ~600 beads were then pipetted onto an inverted glass slide. This concentration was chosen to allow larger wheels to form but prevent very large clusters and interactions between neighboring wheels. To minimize convection due to sample evaporation, a humidifier box (8 cm x 3 cm) was 3-D printed (Form 3, FormLabs) extending the droplet lifetime to hours with addition of a wetted sponge.

Magnetic Field, Imaging and Data Collection. Rotating magnetic fields of field strength 4.5 mT were generated with five 50 mm ID air-cored solenoids, an analog output card (National Instruments (NI), NI-9623, Austin, TX) used to generate sinusoidal signals, and an amplifier (Behringer, EP2000, Willich, Germany) (20). An Olympus OpenStand microscope and a 10x objective (Olympus UPlanApo 10x/0.4) were used to image samples from above in bright field through both glass slide (0.8-1.0 mm) and fluid droplet to paddlebots resting just above the air/water interface. Videos were recorded on a pco.panda 4.2 camera (PCO-TECH Inc., Kelheim, Germany) at 38.67 fps for all μbots except for labeled monomers which were recorded at 80.36 fps.

The number of colloids comprising a µbot was manually counted and recorded. Image analysis software Fiji (21) was used to determine the semi-major axis of a fit ellipse around a µbot which was averaged over an entire trajectory to determine radius. Particle tracking software MuTracker (22) was then used to characterize µbot velocity and rotation rate. Velocities were measured while paddlebots were driven in a square in the flat region at the drop center to ensure no

gravitational effects. To aid image analysis, paddlebot camber angle was kept constant at 30°. Rotation rates were estimated using detrended Fourier transforms of major diameter for asymmetric paddlebots and were manually counted for symmetric paddlebots.

Preparation of labeled beads. To observe and measure monomer rotation rates, beads were sparsely labeled with small polystyrene particles. In this, $100~\mu l$ of stock M-450 solution was dispersed in 40 ml dimethyl sulfoxide (DMSO) to which 80 mg poly(ethylenimine) solution (PEI, Sigma Aldrich, average Mw ~ 2000, 50 wt% in water) was added. After heating at 65 °C for 4 hr, beads were washed with DMSO 3x, ethanol 2x and water 2x and then dispersed in 20 ml DI water. 20 ml of 2 mg/ml polyacrylic acid sodium salt (PAANa, Sigma Aldrich, average Mw ~ 2100, 50 wt% in water solution) was then added. After gentle mixing via rotation at room temperature for 4 hr, beads were washed 3x with DI water. The resulting negatively charge beads were then mixed with positively-charged fluorescent particles (500 nm yellow-green amine group fluorescent polystyrene, Magsphere, Inc.) in 0.1 M NaCl aqueous solution for 2 hr. Unbound particles were removed via subsequent washing with DI water.

Results and Discussion

When subjected to a rotating magnetic field, superparamagnetic particles acquire an attractive dipole and form assemblies whose size distribution depends on the magnetic field strength and initial bead concentration. Once formed, these μ wheels experience a torque due to the rotating field (23) and rotate at a rate ω that follows the applied field at low frequencies but drops as the field frequency reaches the step-out frequency (24). As we have previously shown, spinning μ wheels near liquid/solid interfaces composed of N beads roll at translational velocity $V \propto \omega \cdot N$

due to wet friction with the nearby solid surface (Fig 1A) (7, 25). The beads used in our studies are superparamagnetic due to the presence of iron oxide domains within a polystyrene matrix, resulting in a density significantly greater than water. Being both relatively heavy and only weakly Brownian, gravity drives them towards lower solid surfaces. Near the interface, electrostatic and steric interactions balance gravitational forces and lead to surface separations of order 20-70 nm (8). With addition of salt and/or externally applied fields, it has been shown that this gap has a significant influence on the wet friction and resulting velocities demonstrated by rotating μ wheels. One way of characterizing this interaction is through the traction, effectively a translational efficiency for a rotating μ wheel defined as $V/(\omega R)$, the translational velocity divided by the wheel circumferential velocity. A traction of 1 corresponds to no slip while a μ wheel with 0 traction does not translate.

For studies at the air/water interface, we invert the geometry (Fig 1B) such that the liquid phase containing beads is suspended to create an air/water interface. Here, particles still settle due to gravity but, in the presence of surfactant and following the work of Martinez-Pedrero, *et al.* (26, 27) in their studies of magnetic rollers at the air/water interface, remain suspended in the liquid phase. The film thickness between the beads and the interface can be calculated by balancing the weight of the beads with the electrostatic repulsive forces between the beads and interface (10, 28). For the air/water interface, this film thickness should vary with μ bot size and is estimated to be ~ 50 -60 nm. Supporting this, we observe no evidence of capillary interactions under normal experimental conditions (29, 30). Without added surfactant however, beads do become pinned at the interface (31–33). Once bound, surface tension forces dominate any magnetic forces preventing paddlebots from reorienting out of the interfacial plane and translating. The system

can be further characterized by the Bond number $Bo = \Delta \rho g L^2/\gamma$ where $\Delta \rho$ is the density difference between the water and the beads, g is the acceleration due to gravity, L is the diameter of an individual bead, and γ is the surface tension of water at experimental surfactant concentrations (34). When beads are near the interface and not pinned, we note that such a balance of buoyancy forces against those required to deform the interface due to surface tension (Bo = 3.6•10⁻⁶) suggests that any deviation from a flat interface is minimal.

Upon application of the external rotating magnetic field, µwheels assemble, experience a torque, and rotate as they do near the solid interface. Here however, the differential drag required for directional transport is reversed with the higher drag associated with the paddlebot surface away from the interface leading to velocities in the opposite direction for the same magnetic field rotation. Despite the lack of slip in the traditional sense we still use traction to characterize the nature of paddlebot transport at these fluid surfaces.

In our studies we measure paddlebot velocity, rotation rate, and traction as a function of size, structure, and applied field strength. Guiding our analysis, we expect that the magnetic torque on a paddlebot can be expressed as $\tau = N\nu\mu_o\chi''B^2/\mu^2$ where N is the number of beads, ν the volume of an individual bead, μ_o the permittivity of free space, χ'' the imaginary part of the magnetic susceptibility, and B the magnetic induction field strength (23). Opposing this torque is that due to rotational viscous drag which we approximate with that of a disk $\tau = \frac{32}{3}\eta\omega R^3$ in an unbounded fluid of viscosity η (35). Here we recognize the overall drag and magnitude of the torque will be reduced near the air/water interface; however, we assume the scaling behaviors remain similar. Balancing magnetic and hydrodynamic torques one thus expects $\omega \propto N/R^3$ and

 $V \propto N^2/R^3$. Further approximating paddlebot radius $R \propto N^{1/2}$ leads to $\omega \propto 1/R$ and $V \propto R$. Testing this, we measure velocities and rotation rates of differently-sized paddlebots near the air water interface (Fig 1C). In this, both rotation rate and velocity follow the expected scalings at sizes larger than their individual building blocks; however, and as is apparent in the velocity data, there is spread due to variations in structure in microbots of similar size. Note also the relatively weak dependence of velocity on paddlebot size. At the liquid/solid interface, velocity increases rapidly (Fig. 1C, dashed line) suggesting significantly different tractions at the two interfaces.

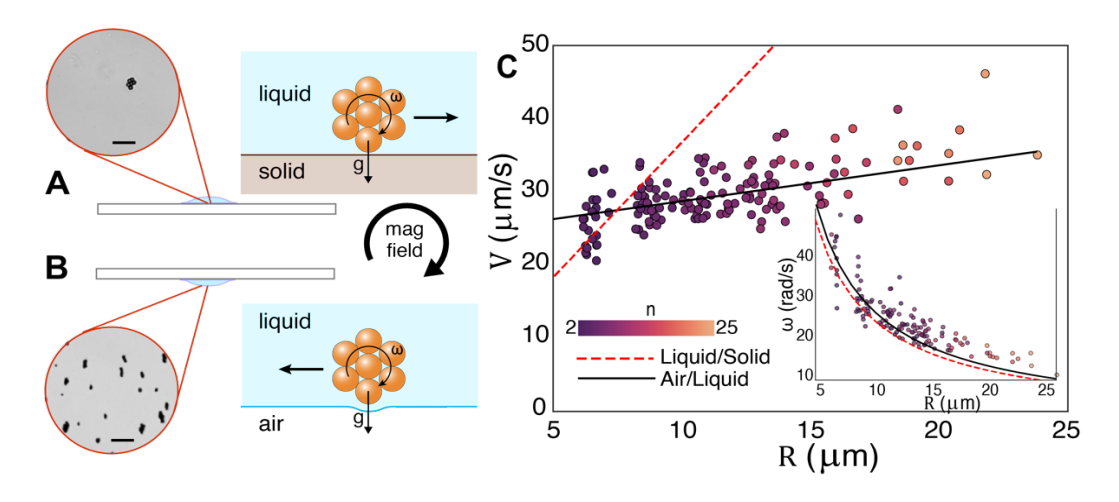


Figure 1. A) Both studies at the liquid/solid and B) air/liquid interfaces use gravity to drive paddlebots towards the interface (scale bar = 25 μm). Note, for a given field rotation, μbots at the air/liquid and liquid solid interfaces translate in opposite directions. C) Measured velocities and rotation rates of paddlebots at the air/water interface at fixed magnetic induction field strength and external rotation field frequency (B = 4.8 mT, $\Omega = 40 \text{ Hz}$). Lines indicate fits to $V \propto R$ and $\omega \propto 1/R$ (inset); dashed line indicates fit to μwheel velocities at the liquid/solid interface. See Supplementary Movie 1.

Paddlebots are assembled under attractive magnetic interactions and form a variety of shapes and sizes. Generally, the higher the initial monomer concentration, the larger the paddlebots that form. Also, paddlebots composed of a certain number of beads can assemble into different trapped shapes of higher energy than the close-packed configuration. Each specific structure can have a different effective circumference and radius of gyration and, as a result and for a fixed field rotation rate, we observe different velocities for particles of identical bead numbers. For µwheels at the liquid/solid interface, interaction with the solid surface and effective traction depends on the µwheel structure. At the air/water interface, we expect similar effects and investigate here traction with paddlebots of different structure (Fig 2).

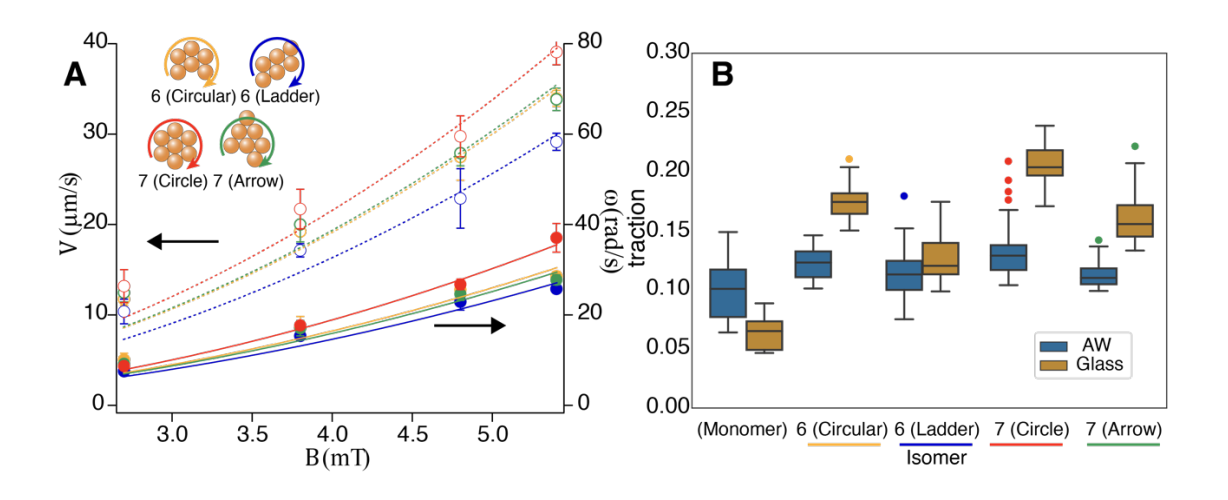


Figure 2 A) Paddlebot velocities (dashed lines) and rotation rates (solid lines) at the air/water interface increase with applied field for different paddlebot structures (6-mer circle yellow measured circularity $\sigma = 0.86$, 7-mer circle red $\sigma = 0.91$, 6-mer ladder blue $\sigma = 0.83$, 7-mer arrow green $\sigma = 0.80$). Fits follow B^2 dependence for both ω and V as predicted by scaling (9 < n < 18) where n is the number of data points per box. B) Tractions are systematically lower at the

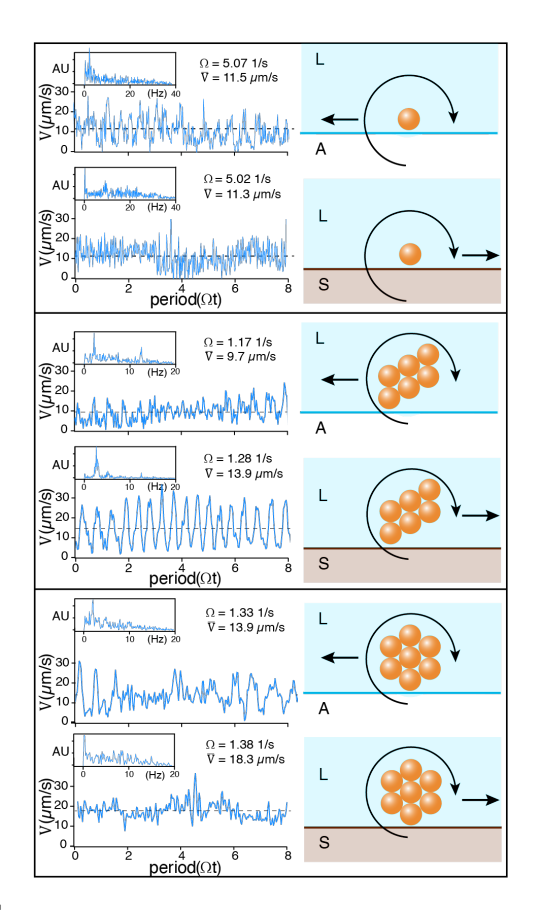
air/water interface than on glass surfaces (7 < n < 15). Monomer rotation tracked via small particle labeling (Supplementary Movie 2). Each distribution of paddlebot isomer tractions is statistically significant from each other with p < 0.05.

In general, tractions are lower for the air/liquid interface than for liquid/solid interfaces (Fig 2B). Despite this, paddlebots of all shapes and sizes can propel themselves at the interface at appreciable rates up to 40 µm/s under the experimental conditions studied here. Importantly, paddlebots must be near the interface – in the bulk they simply spin and do not translate. As discussed previously, the gap between particle and interface plays a significant role in determining the velocity of a rotating bead; translation goes from zero at large separations to increase dramatically as the interface is approached (36). Monomers, representing the unique and structureless case, have higher traction in the air/liquid than in the liquid/solid case (Fig 2B). Here, the gap is determined primarily by a balance of electrostatic and gravitational forces. While we cannot readily measure the gap, under experimental conditions we estimate the surface charge in the water/glass case to be -84 mV (37) vs. -50 mV (38) for the air/water interface. This decrease in charge will lead to a smaller separation, an increase in predicted velocity following (36), and greater tractions in the air/water case. In paddlebots with structure however, we instead observe greater velocities and tractions in the water/solid case where it appears the geometric features on the periphery dominate and additional drag is introduced. Like paddleboats, these features reach into the bulk fluid phase but provide little resistance on that side close to the air/water interface where the fluid drag is significantly reduced.

To quantify, we measure paddlebot instantaneous velocity during translation and rotation (Fig. 3) where the influence of microbot structure becomes apparent. We compare single structureless monomers to a 6-mer "ladder" and a 7-mer "circle"; effectively, the latter two have paddles with the ladder having two/rotation and the circle having six. While fluctuations are apparent in the instantaneous velocity of the monomers both at the air/liquid and liquid/solid interfaces, their translation is smooth. For the structured µbots and in the presence of a solid interface however, we observe cyclic behavior characteristic of proximity of circumferential beads as µwheels rotate, consistent with our previous experimental investigations and theoretical modeling (9). In this, the translational velocity is given a push when the edges of the µwheel are close to the surface where drag is increased and slows down as the fluid gap between µwheel and solid surface increases. At rotation rates that do not provide time to settle, the µwheel center of mass remains at a constant distance from the surface (39, 40). At the air/water interface similar behaviors are observed. Velocity is cyclic and tied to the orientation of anisotropic paddles relative to the interface plane.

As paddlebots become larger and more symmetric the fluctuations due to paddling and differential drag become less noticeable. Comparing air/water to glass as well as paddlebots of different structure we observe distinct behavior. As µwheels rotate, features on the perimeter, specifically the paddles formed from circumferential beads, interact with their surroundings. In the liquid/solid case, propulsion is due to wet friction with the wall. In the air/liquid case, the presence of the air/water interface lowers the effective frictional force available for propulsion, lowering the traction. While the interfacial rheology can be influenced with surfactant or contaminants (41), the reversal in translation direction at the air/water vs. the water/glass

interface, consistent with the calculations of (36), indicates a relatively low-stress air/water interface if not a completely stress-free one. Here, it is the balance of stresses between the bulk and nearby interface that leads to the dominant behaviors in the system. The friction is largest when a paddle is on the bulk liquid side with the higher drag, similar to the macroscopic rowing case. Verifying the periodic nature of the velocity we observe clear peaks in the instantaneous velocity data of twice/period in the ladder case. Showing they are coupled, peaks are also observed at the same frequencies in the ladder instantaneous angle data as confirmed via cross-correlation. Differences in the circle-shaped paddlebots are both expected and observed as 6-mer ladders have two effective paddles/rotation while 7-mer circles have six. We note that, with the additional paddling motion, circles travel faster while ladders are slower with fewer kicks per rotation.



11

Fig 3 – Representative instantaneous velocities measured at the air/liquid and glass interfaces for monomers, ladder-shaped and circle-shaped paddlebots. L = liquid, S = solid, A = air. \overline{V} = mean velocity. Note that, for a given rotation, paddlebots travel in opposite directions at the different surfaces. Insets correspond to Fourier transforms of instantaneous velocity traces. Note, high frequency fluctuations observed for monomers are similar to those measured for beads stuck on a solid surface.

In previous studies, we have shown that similar μ bots can travel up liquid/solid inclines as steep as 80° without use of additional fields (10). Given velocities and tractions that approach those previously demonstrated for liquid/solid interfaces, we test their climbing ability at air/water interfaces in the geometry of Fig. 1B. Here and due to a combination of surface tension and gravitational effects, inverted droplets are flat at the center where our previous measurements have been conducted but approach $\sim 16^{\circ}$ near the edge. Measuring translation velocities up these curved liquid interfaces, the paddling leads to velocities of $\sim 20~\mu\text{m/s}$ under conditions such as those in Fig 1 (Supplemental Movie 3). Interestingly we see relatively little variation of speed with size, similar to the weak dependence observed in Fig. 1C and the subject of future investigations.

Conclusions

We have investigated the motion of colloidal microbots near the air/water interface. In this, the liquid surface provides the necessary symmetry breaking and, due to differential drag, leads to translation and an effective paddling motion that is both directional and rapid. Paddlebot movement is characterized by an oscillatory velocity with maxima associated with higher-drag

configurations. Effective tractions determined by time averaging over these fluctuations suggest that paddlebot motion follows similar trends as for liquid/solid interfaces with microbot structure playing a significant role on the instantaneous velocity characteristics.

Supporting Information

SI Movie 1: Paddlebots of various size translate at different velocities near the air/liquid interface.

SI Movie 2: Sparsely-labeled (bottom) and unlabeled (left) monomers move at similar speeds under the same magnetic field.

SI Movie 3: Paddlebots translating up (towards the bottom) an incline of $\sim 16^{\circ}$.

Acknowledgements

The authors acknowledge support from the National Institutes of Health under grants R21AI138214 and R01NS102465 (C.Z. D.W.M.M.) and the National Science Foundation under grant NSF1762616 (E.V., L.Y., Y.G., D.W.M.M).

References

- 1. Gettelfinger B, Cussler EL (2004) Will humans swim faster or slower in syrup. *AIChE Journal* 50(11):2646–2647.
- 2. Robert Y, Leroyer A, Barré S, Rongère F, Queutey P, Visonneau M (2014) Fluid Mechanics in Rowing: The Case of the Flow Around the Blades. *Procedia Engineering* 72:744–749.
- 3. Ceylan H, Giltinan J, Kozielski K, Sitti M (2017) Mobile microrobots for bioengineering applications. *Lab Chip* 17(10):1705–1724.
- 4. Dong Y, Wang L, Iacovacci V, Wang X, Zhang L, Nelson BJ (2022) Magnetic helical micro-/nanomachines: Recent progress and perspective. *Matter* 5(1):77–109.

- 5. Dreyfus R, Baudry J, Roper ML, Fermigier M, Stone HA, Bibette J (2005) Microscopic artificial swimmers. *Nature* 437(7060):862–865.
- 6. Purcell EM (1977) Life at low Reynolds number. *American journal of physics* 45(1):3–11.
- 7. Tasci TO, Herson PS, Neeves KB, Marr DWM (2016) Surface-enabled propulsion and control of colloidal microwheels. *Nature Communications* 7(1):1–6.
- 8. Disharoon D, Neeves KB, Marr DWM (2019) ac/dc Magnetic Fields for Enhanced Translation of Colloidal Microwheels. *Langmuir* 35(9):3455–3460.
- 9. Yang T, Tomaka A, Tasci TO, Neeves KB, Wu N, Marr DWM (2019) Microwheels on Microroads: Enhanced Translation on Topographic Surfaces. *Sci Robot* 4(32):eaaw9525.
- 10. Zimmermann CJ, Herson PS, Neeves KB, Marr DWM (2022) Multimodal microwheel swarms for targeting in three-dimensional networks. *Sci Rep* 12(1):5078.
- 11. Hu DL, Chan B, Bush JWM (2003) The hydrodynamics of water strider locomotion. *Nature* 424(6949):663–666.
- 12. Hu DL, Bush JW (2005) Meniscus-climbing insects. *Nature* 437(7059):733–736.
- 13. Koh JS, Yang E, Jung GP, Jung SP, Son JH, Lee SI, Jablonski PG, Wood RJ, Kim HY, Cho KJ (2015) BIOMECHANICS. Jumping on water: Surface tension-dominated jumping of water striders and robotic insects. *Science* 349(6247):517–521.
- 14. Danov KD, Kralchevsky PA, Naydenov BN, Brenn G (2005) Interactions between particles with an undulated contact line at a fluid interface: Capillary multipoles of arbitrary order. *Journal of Colloid and Interface Science* 287(1):121–134.
- 15. Danov KD, Kralchevsky PA (2010) Capillary forces between particles at a liquid interface: General theoretical approach and interactions between capillary multipoles. *Advances in Colloid and Interface Science* 154(1-2):91–103.
- 16. Vella D, Mahadevan L (2005) The "Cheerios effect". *American Journal of Physics* 73(9):817–825.
- 17. Shang J, Flury M, Deng Y (2009) Force measurements between particles and the air-water interface: Implications for particle mobilization in unsaturated porous media. *Water Resources Research* 45(6):W06420.
- 18. Scheludko AD, Nikolov D (1975) Measurement of surface tension by pulling a sphere from a liquid. *Colloid and polymer science* 253(5):396–403.
- 19. Fonnum G, Johansson C, Molteberg A, Mørup S, Aksnes E (2005) Characterisation of Dynabeads® by magnetization measurements and Mössbauer spectroscopy. *Journal of Magnetism and Magnetic Materials* 293(1):41–47.
- 20. Roth EJ, Zimmermann CJ, Disharoon D, Tasci TO, Marr DWM, Neeves KB (2020) An experimental design for the control and assembly of magnetic microwheels. *Review of Scientific Instruments* 91(9):093701.
- 21. Schindelin J, Arganda-Carreras I, Frise E, Kaynig V, Longair M, Pietzsch T, Preibisch S, Rueden C, Saalfeld S, Schmid B, Tinevez JY, White DJ, Hartenstein V, Eliceiri K, Tomancak P, Cardona A (2012) Fiji: an open-source platform for biological-image analysis. *Nat Methods* 9(7):676–682.
- 22. Zimmermann CJ (2022) muTracker, DOI:10.5281/zenodo.6459221.
- 23. Maier FJ, Lachner T, Vilfan A, Tasci TO, Neeves KB, Marr DW, Fischer TM (2016) Non reciprocal skewed rolling of a colloidal wheel due to induced chirality. *Soft Matter* 12(46):9314–9320.
- 24. Abbott JJ, Diller E, Petruska AJ (2020) Magnetic methods in robotics. *Annual Review of Control, Robotics, and Autonomous Systems* 3(1):57–90.

- 25. Zimmermann CJ, Schraeder T, Reynolds B, DeBoer EM, Neeves KB, Marr DWM (2022) Delivery and actuation of aerosolized microbots. *Nano Select* 3(7):1185–1191.
- 26. Martinez-Pedrero F, Ortiz-Ambriz A, Pagonabarraga I, Tierno P (2015) Colloidal Microworms Propelling via a Cooperative Hydrodynamic Conveyor Belt. *Physical Review Letters* 115(13):138301.
- 27. Martín-Roca J, Jiménez M, Ortega F, Calero C, Valeriani C, Rubio RG, Martínez-Pedrero F (2022) Rotating Micro-Spheres for adsorption monitoring at a fluid interface. *J Colloid Interface Sci* 614:378–388.
- 28. Du Y, Bradford SA, Shen C, Li T, Bi X, Liu D, Huang Y (2022) Novel analytical expressions for determining van der Waals interaction between a particle and air-water interface: Unexpected stronger van der Waals force than capillary force. *J Colloid Interface Sci* 610:982–993.
- 29. Kralchevsky PA, Paunov VN, Denkov ND, Ivanov IB, Nagayama K (1993) Energetical and force approaches to the capillary interactions between particles attached to a liquid-fluid interface. *Journal of colloid and interface science* 155(2):420–437.
- 30. Kralchevsky PA, Nagayama K (1994) Capillary forces between colloidal particles. *Langmuir* 10(1):23–36.
- 31. Guzmán E, Martínez-Pedrero F, Calero C, Maestro A, Ortega F, Rubio RG (2022) A broad perspective to particle-laden fluid interfaces systems: from chemically homogeneous particles to active colloids. *Adv Colloid Interface Sci* 302:102620.
- 32. Naga A, Butt HJ, Vollmer D (2021) The Force Required to Detach a Rotating Particle from a Liquid-Fluid Interface. *Langmuir* 37(44):13012–13017.
- 33. Nutt CW (1960) Froth flotation: The adhesion of solid particles to flat interfaces and bubbles. *Chemical Engineering Science* 12(2):133–141.
- 34. Correia EL, Brown N, Ervin A, Papavassiliou DV, Razavi S (2022) Contamination in Sodium Dodecyl Sulfate Solutions: Insights from the Measurements of Surface Tension and Surface Rheology. *Langmuir* 38(23):7179–7189.
- 35. Jeffery GB (1915) On the Steady Rotation of a Solid of Revolution in a Viscous Fluid. *Proceedings of the London Mathematical Society* s2 14:327–338.
- 36. Lee SH, Leal LG (1980) Motion of a sphere in the presence of a plane interface. Part 2. An exact solution in bipolar co-ordinates. *Journal of Fluid Mechanics* 98(1):193–224.
- 37. Gu Y, Li D (2000) The ζ-Potential of Glass Surface in Contact with Aqueous Solutions. *Journal of Colloid and Interface Science* 226(2):328–339.
- 38. Jia W, Ren S, Hu B (2013) Effect of water chemistry on zeta potential of air bubbles. *Int J Electrochem Sci* 8(4):5828–5837.
- 39. Zhang L, Petit T, Lu Y, Kratochvil BE, Peyer KE, Pei R, Lou J, Nelson BJ (2010) Controlled Propulsion and Cargo Transport of Rotating Nickel Nanowires near a Patterned Solid Surface. *ACS Nano* 4(10):6228–6234.
- 40. Sing CE, Schmid L, Schneider MF, Franke T, Alexander-Katz A (2010) Controlled surface-induced flows from the motion of self-assembled colloidal walkers. *Proc Natl Acad Sci U S A* 107(2):535–540.
- 41. Bos MA, Van Vliet T (2001) Interfacial rheological properties of adsorbed protein layers and surfactants: a review. *Advances in Colloid and Interface Science* 91(3):437–471.

TOC Graphic

